

Accepted Manuscript

A kinetic comparison between E2P and the E2P-like state induced by a beryllium fluoride complex in the Na,K-ATPase. Interactions with Rb⁺

Santiago Enrique Faraj, Mercedes Centeno, Rolando Carlos Rossi, Mónica Raquel Montes



PII: S0005-2736(18)30319-5

DOI: <https://doi.org/10.1016/j.bbamem.2018.10.020>

Reference: BBAMEM 82881

To appear in: *BBA - Biomembranes*

Received date: 26 June 2018

Revised date: 24 October 2018

Accepted date: 30 October 2018

Please cite this article as: Santiago Enrique Faraj, Mercedes Centeno, Rolando Carlos Rossi, Mónica Raquel Montes, A kinetic comparison between E2P and the E2P-like state induced by a beryllium fluoride complex in the Na,K-ATPase. Interactions with Rb⁺. *Bbamem* (2018), <https://doi.org/10.1016/j.bbamem.2018.10.020>

This is a PDF file of an unedited manuscript that has been accepted for publication. As a service to our customers we are providing this early version of the manuscript. The manuscript will undergo copyediting, typesetting, and review of the resulting proof before it is published in its final form. Please note that during the production process errors may be discovered which could affect the content, and all legal disclaimers that apply to the journal pertain.

A kinetic comparison between E2P and the E2P-like state induced by a beryllium fluoride complex in the Na,K-ATPase. Interactions with Rb⁺

Santiago Enrique Faraj, Mercedes Centeno, Rolando Carlos Rossi, Mónica Raquel Montes*

Universidad de Buenos Aires, Facultad de Farmacia y Bioquímica, Departamento de Química Biológica and Consejo Nacional de Investigaciones Científicas y Técnicas (CONICET)–Universidad de Buenos Aires, Instituto de Química y Fisicoquímica Biológicas (IQUIFIB). Buenos Aires, Argentina.

*To whom correspondence should be addressed: Mónica R. Montes: Departamento de Química Biológica, Facultad de Farmacia y Bioquímica, Universidad de Buenos Aires, Junín 956, 1113 Buenos Aires, Argentina; mmontes@qb.ffyb.uba.ar; Tel. (+54) 011 4964-8289; Fax. (+54) 011 4962-5457.

ABSTRACT

Metal-fluoride complexes have been used to induce E2P-like states with the aim of studying the events that occur during E2P hydrolysis in P-type ATPases. In the present work, we compared the E2P-like state induced by a beryllium fluoride complex (BeF_x) with the actual E2P state formed through backdoor phosphorylation of the Na,K-ATPase. Formation of E2P and E2P-like states were investigated employing the styryl dye RH421. We found that BeF_x is the only fluorinated phosphate analog that, like Pi, increases the RH421 fluorescence. The observed rate constant, k_{obs} , for the formation of E2P decreases with [Pi] whereas that of E2BeF_x increases with [BeF_x]. This might wrongly be taken as evidence of a mechanism where the binding of BeF_x induces a conformational transition. Here, we rather propose that, like for Pi, binding of BeF_x follows a conformational-selection mechanism, i.e. it binds to the E2 conformer forming a complex that is much more stable than E2P, as seen from its impaired capacity to return to E1 upon addition of Na^+ . Although E2P and E2BeF_x are able to form states with 2 occluded Rb^+ , both enzyme complexes differ in that the affinity for the binding and occlusion of the second Rb^+ is much lower in E2BeF_x than in E2P. The higher rates of Rb^+ occlusion and deocclusion observed for E2BeF_x , as compared to those observed for other E2P-like transition and product states suggest a more open access to the cation transport sites, supporting the idea that E2BeF_x mimics the E2P ground state.

Keywords: Na,K-ATPase, conformational change, enzyme mechanism, enzyme kinetics, membrane transport, phosphorylated states, ligand binding kinetics, Rb^+ occlusion and deocclusion.

1. Introduction

Na,K-ATPase is a prominent member of the P-type ion-transporting ATPases, responsible for generating electrochemical gradients of Na^+ and K^+ across the plasma membrane. It comprises an α and a β subunit and a protein belonging to the FXYD family is often associated. The α subunit presents 10 hydrophobic membrane-spanning helices in which cation binding sites are located, and three cytoplasmic domains (A, P and N) where ATP binding and enzyme phosphorylation and dephosphorylation occur. During the transport cycle (Fig. 1), the enzyme undergoes cyclical conformational changes between two main reaction states, E1 and E2, and their phosphorylated forms, E1P and E2P. The E1 conformation binds intracellular Na^+ and ATP to form the E1P(Na_3) state. After a conformational transition to E2P, Na^+ is released and K^+ binding from the extracellular side leads to a rapid dephosphorylation and occlusion of the cation producing E2(K_2). Finally, K^+ is released into the cytosol after the binding of ATP to a low affinity site [1].

P-type ATPases share a common phosphorylation and dephosphorylation mechanism; the reactions of ATP binding, phosphoryl transfer and hydrolysis, and the mechanical transduction of the energy released in this process to the ion-binding site, are highly conserved [1]. The physiological pathway of dephosphorylation has been postulated to occur through a series of consecutive states, each one with a different kind of interaction between the phosphoryl group and the enzyme: E2-P (E2P ground state) \rightarrow E2·P (E2P transition state) \rightarrow E2·Pi (E2P product state) \rightarrow E2 + Pi. In the Na,K-ATPase, the reaction sequence during dephosphorylation due to K^+ binding (enclosed in gray in Fig. 1) leads from a non-occluded state, E2PK₂, to one in which ions become occluded, E2(K₂). As it is shown in the model, E2P might be formed through the ATP-dependent physiological route or by the direct incorporation of Pi through the so-called backdoor phosphorylation.

Metal-fluoride complexes and vanadate inhibit ATPase activity and have been used to induce E2P-like states that mimic the ground (E2BeF_x), transition (E2AlF_x and E2-vanadate) and product (E2MgF_x) states [2-8]. These complexes have also been of use for obtaining crystal structures of various P-type ATPases [5-8]. The sarco(endo)plasmic reticulum Ca^{2+} -ATPase (SERCA) has been crystallized in several states thus allowing the description of almost every intermediate of the catalytic cycle and studies

in pig gastric H,K-ATPase describe structures of MgF_x -bound, BeF_x -bound and AlF_x -bound conformations [9, 10]. Regrettably, in terms of metal-fluoride phosphate analogs that mimic E2P-like states, Na,K-ATPase has only been crystallized in the $\text{E2MgF}_4(\text{Rb}_2)$ state.

The case of the sodium pump is particularly interesting since its dephosphorylation reaction is associated with K^+ binding and transport. Here, we test the hypothesis that each intermediate in the sequence of phosphorylated states (ground, transition and product states) is related to a difference in the kinetics of occlusion and deocclusion of K^+ . The technique developed in our laboratory makes it possible to isolate and quantify the intermediates containing occluded cations in the millisecond time scale [11]. Previous results from our laboratory have shown a functional characterization of the occlusion of Rb^+ (as a K^+ -congener) in the E2Mg -vanadate [12] and E2Mg-MgF_4 states [13].

In this work, we assess the properties of the E2P-like state induced by BeF_x (E2BeF_x) and compare them with those of the actual E2P state formed by P_i backdoor phosphorylation. We investigate the mechanism underlying the formation of these states by measuring the kinetics of the $\text{E1} \leftrightarrow \text{E2}$ conformational change and the appearance of E2P and E2BeF_x . For this, we analyzed the effects of P_i and BeF_x on the Na,K-ATPase fluorescence changes reported by the probes eosin and RH421. Results of Rb^+ occlusion in E2P and E2BeF_x , obtained in equilibrium and transient experiments, were analyzed using a model to describe and compare the observed behavior. Our results provide functional information that matches the structure proposed for the E2P ground state in other P-type ATPases.

2. Materials and Methods

2.1 Enzyme conditions

Na,K-ATPase, partially purified from pig kidney according to Klodos, Esmann and Post [14], was kindly provided by the Department of Biophysics of the University of Århus in Denmark. The specific activity at the time of preparation was 23–25 (μmol of P_i) min^{-1} (mg of protein) $^{-1}$ measured under optimal conditions (150 mM NaCl, 20 mM KCl, 3 mM ATP, and 4 mM MgCl_2 in 25 mM imidazole-HCl, pH 7.4 at 37 °C). The maximum number of nucleotide sites in the preparations used in this work was

2.2–2.6 nmol (mg protein)⁻¹; this corresponds to a maximum of 4.4–5.6 nmol of occluded Rb⁺ per mg of protein.

2.2 Reagents

[⁸⁶Rb]RbCl (⁸⁶Rb⁺) was obtained from Perkin-Elmer NEN Life Sciences (USA). The fluorescent probes eosin-Y (eosin) and *N*-(4-Sulfobutyl)-4-(4-(*p*-(dipentylamino)phenyl)butadienyl)-pyridinium salt (RH421), as well as BeSO₄ and NaF were from Sigma Chemical Co (USA). Phosphate and fluoride were obtained as imidazolium salts (Pi and ImF), by passing the solutions through a column containing the cation exchange AG MP50 resin (BioRad) previously equilibrated with imidazole. All other reagents were of analytical grade.

2.3 Reaction conditions

All incubations were performed at 25 °C in media containing 25 mM imidazole-HCl (pH 7.4 at 25 °C) and 0.25 mM EDTA. In the presence of Pi, experiments measuring E2P formation contained 3 mM MgCl₂ whereas for Rb⁺ occlusion the media contained 0.5 mM MgCl₂, which is enough to shift the equilibrium to E2P. Experiments with Be²⁺ + F⁻ contained 0.3 mM MgCl₂ in order to prevent the formation of Mg²⁺ + F⁻ complexes. The concentration of free Mg²⁺ can be estimated as [MgCl₂] – [EDTA] – [other complexes], depending on the particular composition of the medium. The concentration of BeF₃⁻ was calculated from the total concentration of beryllium and fluoride according to Mesmer and Baes [15]. In the experiments measuring occluded Rb⁺, the levels of Be²⁺, BeF⁺, and BeF₄³⁻ are 0.014, 2.0, and 1.25 μM, respectively, whereas those of BeF₂, BeF₃⁻, and F⁻ are 21.7 μM, 25.0 μM, and 1.87 mM, respectively. The concentrations of other components are indicated in each figure legend.

2.4 Conformational changes

The conformational states of the Na,K-ATPase were studied by measuring the eosin fluorescence signal which is high for states in E1 and is low for states in E2 [16, 17]. Enzyme preparation (40 μg of protein per ml) was incubated with 0.4 μM eosin. Equilibrium measurements were carried out in a Jasco FP-6500 spectrofluorometer. The excitation and emission wavelengths were 520 and 540 nm, respectively, with a band-pass of 3 nm. RH421 detects the formation of acid-stable phospho-enzyme

(E2P) formed by Pi [18]. We measured the time courses of E2P formation in a medium with 45 μg of protein per ml and 0.3 μM RH421.

Measurements of the time course of fluorescence were performed with a stopped-flow reaction analyzer (SX-18MV, Applied Photophysics). In each experiment, 2000 data points were collected. Between 5 and 7 experimental traces were averaged to evaluate each time course. When the enzyme incubated with RH421 was mixed with buffer, a slow, nonspecific increase in fluorescence was observed as a function of time, which is represented by the linear component in the fitting equation (see Equation 1). For eosin assays, the excitation wavelength was 520 nm, and emitted light was filtered through an OG550 filter (Schott Advanced Optics). For RH421 experiments, the excitation wavelength was 546 nm, and emitted light was filtered through an RG645 filter (Schott Advanced Optics).

2.5 Occluded Rb^+

$^{86}\text{Rb}^+$ occlusion was measured according to Rossi, Kaufman, Gonzalez Lebrero, Norby and Garrahan [11]. Briefly, reactions were carried out in a rapid-mixing apparatus (SFM4 from Bio-Logic, France) connected to a quenching and washing chamber that contained a *Millipore* filter. The filter was then removed, dried, and counted for radioactivity. Blanks were estimated from the amount of $^{86}\text{Rb}^+$ retained in the filters when the enzyme was omitted. Equilibrium occlusion of Rb^+ was attained by incubating enzyme during at least 20 min. The time course of Rb^+ occlusion was measured after mixing one volume of enzyme suspension with one volume of a solution containing $^{86}\text{Rb}^+$ and incubated for different lengths of time. To measure the time course of Rb^+ deocclusion, one volume of enzyme suspension equilibrated with a certain [$^{86}\text{Rb}^+$] (0.03–5.00 mM) was mixed with 19 volumes of a solution containing an identical concentration of unlabeled Rb^+ as to cause a 20-fold decrease in the specific activity of $^{86}\text{Rb}^+$. Regarding the media composition, the levels of Be^{2+} , BeF^+ , and BeF_4^{3-} are negligible in our experimental conditions. BeF_2 at 20 μM and about 1.9 mM of F^- do not seem candidates to modify cation occlusion in a reaction medium with 0.3 mM MgCl_2 and 25 mM Cl^- .

2.6 Data analysis

The equations were fitted to the experimental data by a nonlinear regression procedure using *OriginPro 2017*. When necessary, to discriminate between several equations that fitted similarly well the experimental results, we used the second-order Akaike Information Criterion (AIC_C) [19]; the best equation was chosen as that giving the lower value of AIC_C. Parameters are expressed as value ± standard error (S.E.). To fit the kinetic model to experimental data we used the freeware program *COPASI 4.20* [20]. In order to reduce the variability of the fitted rate constants, we applied temporary constraints on some of them. Specifically, we used values of on-rate constants between 1 and 500 μM⁻¹ s⁻¹.

3. Results and discussion

3.1 Fluorescence changes associated with Pi and BeF_x binding

We compared the ability of Pi and beryllium fluoride to induce the formation of the E2P and E2BeF_x states in the Na,K-ATPase, employing fluorescence measurements of eosin to evaluate the E1↔E2 conformational change and of RH421 to assess the formation of E2P-like states. Fig. 2 shows that, in media with Mg²⁺, the high eosin fluorescence signal (associated to the E1 conformation) decreases upon the addition of Pi and Be²⁺ + F⁻. Under equilibrium conditions the signal drop with [Pi] and [BeSO₄] can be described by the equation $Y=Y_0 K_{0.5}/(X+K_{0.5})$, where Y is the normalized fluorescence value and X is the ligand concentration. The best-fitting value of K_{0.5} for Pi was 295 ± 14 μM, whereas K_{0.5} for BeSO₄ in media with 2 mM fluoride was 0.28 ± 0.04 μM. At 100 μM BeSO₄, the decrease with fluoride concentration was sigmoid, as expected for a binding stoichiometry of over one F⁻ per Be²⁺, and was well described by the equation $Y=Y_0 K_{0.5}^n/(X^n+K_{0.5}^n)$, where the best-fitting values of n and K_{0.5} were 3.1 ± 0.2 and 389 ± 11 μM, respectively. It is worth mentioning that crystallographic studies indicate that BeF₃⁻ is the chemical species that form stable complexes with P-type ATPases [21].

Although the fluorescent probe RH421 has been used to detect both ATP and Pi-dependent formation of E2P states in the Na,K-ATPase [22-26], its use to monitor E2P-like states (other than E2P itself) is poorly documented, with the exception of E2-vanadate in shark enzyme [23]. In Fig. 3 we show the kinetics of fluorescence changes of RH421 induced by Pi, vanadate and metal-fluoride complexes of

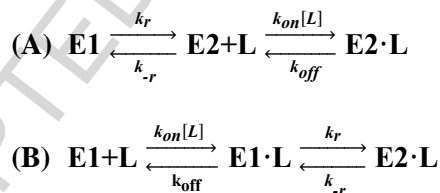
Mg^{2+} , Al^{3+} and Be^{2+} . It can be seen that, as Pi, BeF_x significantly increases the RH421 signal, probably by the formation of an E2BeF_x state. It is also possible to observe a small increase in the presence of vanadate, while aluminum and magnesium fluorides complexes do not produce any significant change.

In order to evaluate the mechanism of Pi and BeF_x binding to the protein, a volume of enzyme with Mg^{2+} was mixed with a volume of a solution containing increasing concentrations of Pi or of Be^{2+} in the presence of F^- (Fig. 4). The fluorescence time courses were satisfactorily described by an exponential function of time plus an increasing linear component (see 2.4 Conformational changes):

$$F(t) = F_0 + F_1 (1 - e^{-k_{obs} t}) + m t \quad \text{Eq. 1}$$

where F_0 and F_1 are the amplitudes of the fast and slow phases, respectively, k_{obs} is the observed rate constant and m is the slope of the linear component.

Fig. 5 shows the values of k_{obs} as a function of the concentration of Pi and BeF_3^- . It can be seen that k_{obs} decreases with [Pi], as previously described for the shark enzyme [24, 27], and increases with $[\text{BeF}_3^-]$. These results can be interpreted on the basis of the mechanisms shown in Scheme 1, where L stands for Pi or BeF_3^- .



Scheme 1: Conformational-selection (A) and induced-fit (B) mechanisms of ligand binding. k_i s are rate constants.

Assuming rapid equilibrium for the binding of both ligands, these results suggest a conformational-selection mechanism for Pi [23] and an induced-fit mechanism for the binding of BeF_3^- [28]. However, Vogt and Di Cera [29] showed that if the rapid-equilibrium assumption is not held, and given certain relationships between rate constants, a conformational-selection mechanism can be wrongly taken as an induced-fit one when k_{obs} increases with the ligand concentration.

According to the set of differential equations associated with the conformational-selection mechanism (A in Scheme 1) the observed rate constant, k_{obs} , is expressed by:

$$k_{obs} = \frac{k_r + k_{-r} + k_{off} + k_{on}[L] - \sqrt{(k_{off} + k_{on}[L] - k_r - k_{-r})^2 + 4 k_{-r} k_{on} [L]}}{2} \quad \text{Eq. 2}$$

It should be noted that the mechanisms in Scheme 1 predict two phases for approaching equilibrium but detection of the contribution of the fast component may be difficult with standard transient kinetics and may require the use of ultrarapid techniques like continuous flow and temperature jump [29]. The smaller rate coefficient, k_{obs} in Equation 2, defines the evolution of the system over a time scale accessible to rapid kinetics techniques like stopped flow.

Equation 2 predicts that in a conformational-selection mechanism, as $[L]$ increases, k_{obs} might increase or decrease, approaching the asymptotic value of k_r . The limit for $[L] = 0$ defines a value of k_{obs} equal to: (a) $k_{-r} + k_r$ when $k_{off} > k_{-r} + k_r$, and to (b) k_{off} when $k_{off} < k_{-r} + k_r$. Decreasing values of k_{obs} when $[L]$ increases is always evidence of a conformational-selection mechanism. However, if $k_{off} < k_r$, it can be shown that k_{obs} will be an increasing function of $[L]$.

From the results in Fig. 5A and as predicted by the Albers-Post model, the binding of Pi follows a conformational-selection mechanism. Therefore, the same mechanism may be expected for the binding of phosphate analogs that stabilize the E2 conformer. If this were true, under similar experimental conditions the values of k_r and k_{-r} should be relatively independent of the ligand that binds to E2. With this in mind, Equation 2 was fitted separately to the data in Fig. 5 (continuous lines) or globally fitted, i.e. including both sets of data and using shared values of k_r and k_{-r} (dashed lines). Best fitting values are shown in Fig. 5. It can be seen that when separately fitted, Equation 2 provides a good description to the results of k_{obs} as a function of both $[Pi]$ and $[BeF_3^-]$, and (with some bias) so does the global fitting. In this work we do not intend a detailed quantitative analysis; our results, however, show that the same mechanism can account for the effects of both Pi and BeF_3^- . In this sense, note that the values of k_r , i.e. the rate constant of the E1→E2 conformational transition (k_{obs} at $[L] \rightarrow \infty$), lie between 0.1 and 0.2 s⁻¹. A similar value of about 0.3 s⁻¹ was obtained by addition of a non-limiting concentration of vanadate [12]. When fitting independently the data for Pi and BeF_3^- , some difference in the values of k_r and k_{-r} can be expected since the experimental conditions are different, like for instance the concentration of Mg²⁺ and the presence or the absence of fluoride and beryllium. However, the use of a single set of values of k_r and k_{-r} for both

ligands, qualitatively predicts the observed behavior. Values of k_{on} and k_{off} are very poorly estimated (their standard error values are very large) for the case of Pi, probably because the binding of Pi to E2 is a rapid-equilibrium step. On the other hand, the low value of k_{off} found for BeF_3^- (the ordinate value in Fig. 5B) is incompatible with a rapid-equilibrium binding and would be in agreement with a much higher affinity of E2 for BeF_x than for Pi.

The preconception for assigning an induced-fit mechanism for the interactions between the enzyme and BeF_x probably lies on (i) the increase in the observed rate constant with the ligand concentration, and (ii) the rapid-equilibrium assumption for the binding step, which might be wrong. It can be shown that, k_{obs} for $[\text{L}] \rightarrow \infty$ for an induced-fit mechanism (Scheme 1B), approaches $k_{-r} + k_r$, i.e. the sum of rate constants for the $\text{E1L} \rightleftharpoons \text{E2L}$ conformational transition subsequent to the binding step [29]. As there is no *a priori* theoretical restriction for the values of k_{-r} and k_r in an induced-fit mechanism, a conformational-selection mechanism seems a simpler explanation for the similarity in the values of k_{obs} for $[\text{L}] \rightarrow \infty$ found for Pi, BeF_x and vanadate.

In accordance with the value estimated for k_{off} (see table in Fig. 5) we found that Na^+ is capable of counteracting the effect of Pi, but not the one exerted by BeF_x . We used eosin fluorescence to investigate the effect of Na^+ to induce a conformational change from E2P or E2BeF_x to E1. Results in Fig. 6 show that, unlike the case of Pi, Na^+ is unable to bring E2BeF_x to E1 in the time length of the experiment. Taking for granted that both Pi and BeF_x share the same mechanism, the rate-limiting step would be given by the release of BeF_x .

3.2 Rb^+ occlusion by E2P and E2BeF_x

To compare the behavior of E2P and E2BeF_x as regards cation binding and occlusion, we investigated their ability to occlude Rb^+ in equilibrium and transient experiments.

3.2.1 Equilibrium conditions

Fig. 7 shows the level of occluded Rb^+ (Rb_{occ}) measured in equilibrium conditions as a function of $[\text{Rb}^+]$. Results could be described by a rational function:

$$Rb_{occ} = \frac{Occ_1 K_{Rb2} [Rb^+] + Occ_2 [Rb^+]^2}{K_{Rb1} K_{Rb2} + K_{Rb2} [Rb^+] + [Rb^+]^2} \quad \text{Eq. 3}$$

where the exponent 2 is related to the maximum number of Rb^+ ions occluded per enzyme unit, Occ_1 and Occ_2 are maximal levels of Rb_{occ} and K_{Rb1} and K_{Rb2} are apparent dissociation constants.

When occlusion experiments were performed in the presence of Pi , equilibrium values of Rb_{occ} increased along a saturable, slightly sigmoid curve that presents a positive slope at $[Rb^+] \rightarrow 0$ (see inset in Fig. 7A). Equation 3 was fitted to the results, the best fitting values of the parameters were: $Occ_1 = 2.23 \pm 0.90 \text{ nmol } Rb^+ (\text{mg protein})^{-1}$, $Occ_2 = 4.47 \pm 0.08 \text{ nmol } Rb^+ (\text{mg protein})^{-1}$, $K_{Rb1} = 0.05 \pm 0.02 \text{ mM}$ and $K_{Rb2} = 0.04 \pm 0.01 \text{ mM}$. These values agree with the idea that in E2P the occlusion of one Rb^+ facilitates the binding and occlusion of the second cation, thus explaining the observed sigmoidicity. A sigmoid shape was also reported by Gonzalez-Lebrero, Kaufman, Garrahan and Rossi [30] in media with 5 mM $MgCl_2$, and by Cornelius, Fedosova and Klodos [27] measuring the change in RH421 fluorescence as a function of $[K^+]$, both for shark-rectal and pig-renal enzyme.

In the presence of Be^{2+} and F^- in concentrations enough as to bring most of the enzyme to the $E2BeF_x$ state (Fig. 7B), Rb_{occ} increases with the concentration of the cation along a curve that displays two components, one with high and one with low apparent affinity. Equation 3 was fitted to results in Fig. 7B. Due to the difficulty to reach saturation, the amount of Rb_{occ} at $[Rb^+] \rightarrow \infty$ (Occ_2) was set at $4.5 \text{ nmol } Rb^+ (\text{mg protein})^{-1}$, which is close to the maximal capacity of occlusion of this enzyme preparation. With this constraint, the best fitting values were: $Occ_1 = 1.65 \pm 0.10 \text{ nmol } Rb^+ (\text{mg protein})^{-1}$, $K_{Rb1} = 0.033 \pm 0.006 \text{ mM}$ and $K_{Rb2} = 6.5 \pm 0.8 \text{ mM}$. The low affinity component, whose value of K_{Rb2} is more than 100-fold higher than that found for E2P (cf. 6.5 mM vs. 0.04 mM), was not observed in other E2P-like states, like those induced by vanadate [12] or magnesium fluoride [13], and shows the difficulty for binding/occlusion of the second Rb^+ to $E2BeF_x$. As for the high apparent affinity component, which is due to forms containing a single occluded Rb^+ , the value of Occ_1 is lower than that of $Occ_2/2$ probably because the equilibrium between species with one bound Rb^+ and one occluded Rb^+ is not sufficiently shifted towards the latter.

From a general point of view, the occlusion of Rb^+ by E2P and E2BeF_x displays positive and negative cooperativities, respectively.

3.2.2 Kinetics of Rb^+ exchange

Several works have reported that Pi accelerates the release of Rb^+ or K^+ from the occluded state of the Na,K-ATPase [31-33]. Nevertheless, we have shown that the compounds used to imitate the phosphoryl group in the transition (vanadate) and product (magnesium fluoride) states do not increase the rate of Rb^+ deocclusion [12, 13]. Here, we assessed the release of Rb^+ from the occluded state of the enzyme formed with beryllium fluoride, $\text{E2BeF}_x(\text{Rb}_n)$, where n can be 1 or 2. Fig. 8 shows the decrease of Rb_{occ} with time for the inhibited complex or for a control without BeF_x . Direct experimental evidence that the release of Rb^+ from the Na,K-ATPase in the E2 conformation takes place through the extracellular access was given by Forbush [34] and by Karlisch and Stein [35] using sided preparations. Based on the Albers-Post model and on kinetics of Rb^+ deocclusion, González Lebrero *et al.* [30] also found—in a non-compartmentalized preparation—strong evidence that the occluded state formed in the absence of added ligands, $\text{E2}(\text{Rb}_2)$, mainly exchanges Rb^+ through the extracellular side of the pump (see also references [32, 36, 37]). Therefore, the experiment in Fig. 8, evaluates Rb^+ release to this side for the control and inhibited enzyme. The results were analyzed by fitting the sum of two exponential functions of time plus a constant term:

$$\text{Rb}_{\text{occ}} = A_1 e^{-k_1 t} + A_2 e^{-k_2 t} + A_\infty \quad \text{Eq. 4}$$

where A_1 and k_1 , and A_2 and k_2 correspond to the amplitudes and observed rate coefficients of the fast and slow phases, respectively, and A_∞ is the value of Rb_{occ} when $t \rightarrow \infty$. Best fitting values of rate coefficients were: (s^{-1}) $k_1 = 0.06 \pm 0.04$ and $k_2 = 0.005 \pm 0.025$ in the absence, and $k_1 = 0.6 \pm 0.2$ and $k_2 = 0.035 \pm 0.007$ in the presence of BeF_x , indicating that $\text{E2BeF}_x(\text{Rb}_n)$ presents a higher velocity of Rb^+ release. Note that a similar experiment performed in the presence of Pi gives, respectively, values of k_1 and k_2 of about 30 and 2 s^{-1} , in agreement with previous reports [30, 32].

In order to characterize the release of Rb^+ from $\text{E2BeF}_x(\text{Rb}_n)$ we performed experiments for Rb^+ concentrations ranging from 0.03 to 5 mM (Fig. 9). It is clear that Rb^+ is released along a biphasic time

course. Fitting of Equation 4 to the values of Rb_{occ} as a function of time yielded the parameter values plotted in Fig. 9, *B* and *C*. Unlike it was reported for experiments performed in the presence of Pi [30, 32] where A_1 and A_2 were similar, we found that the amplitude of the slow component is always smaller than that of the fast one, i.e. $A_2 < A_1$, and that both values tend to be equal as $[Rb^+]$ increases (Fig. 9*B*). While values of k_l lie between 0.1 and 0.3 s⁻¹, the velocity of the slow phase (mainly represented by k_2) seems to decrease with $[Rb^+]$ with low affinity. This behavior may be interpreted as a blockage effect exerted by the Rb^+ present in the medium [32, 33], as we will show below.

To investigate the binding and occlusion of Rb^+ by E2P and E2BeF_x, we measured the time course of occlusion at different Rb^+ concentrations. The results are given in Fig. 10. Best fit to each of the curves was attained by a monoexponential function of time plus a constant term:

$$Rb_{occ} = A_0 + A_1 (1 - e^{-k_{occ} t}) \quad \text{Eq. 5}$$

where A_0 represents the maximal occlusion level of a very fast component, and A_1 and k_{occ} are the amplitude and observed rate coefficient of the slower component, respectively.

The best fitting values of parameters from Equation 5 are plotted in Fig. 10, panels *B* and *C* for Pi and panels *E* and *F* for BeF_x. The figure shows that the increase in A_1 with $[Rb^+]$ displays a low-affinity component for the case of E2BeF_x but not for E2P (cf. panels *B* and *E*), which is related to the equilibrium results in Fig. 7. In the presence of Pi, the values of k_{occ} show a marginal, saturable increment with $[Rb^+]$, whereas, in the case of BeF_x, the tendency becomes uncertain due to the magnitudes of the standard errors. As the addition of Rb^+ should produce the dephosphorylation of E2P, the increment of k_{occ} is compatible with results obtained by Cornelius, Fedosova and Klodos [27], who observed an increase of k_{obs} with $[K^+]$ from 0.02 to 0.04 s⁻¹ measuring RH421 fluorescence change.

The occlusion of Rb^+ by E2P and by E2BeF_x is very slow as compared to the rate observed for E2P formed with ATP (cf. with results from Kaufman, Gonzalez-Lebrero, Rossi and Garrahan [38]). These results are in agreement with the observation that the E2P state formed by the backdoor phosphorylation, in the absence of alkali cations, is kinetically different from that formed by the physiological route [27,

39, 40] in that the dephosphorylation of the former is rather insensitive to the addition of K^+ and its congeners.

It seems interesting to note that the rates of Rb^+ occlusion and deocclusion in the presence of BeF_x are higher than those observed for the complexes of the enzyme with $Mg^{2+} + F^-$ (E2P product state) and with vanadate (E2P transition state), suggesting the existence of a more open extracellular access to the cation sites [12, 13]. These results agree with the idea that $E2BeF_x$ mimics the E2P ground state, in accordance with the open luminal structure found for the $E2BeF_3$ complex of SERCA1a [41], which, according with Yatime, Laursen, Morth, Esmann, Nissen and Fedosova [42], is closely related to the ouabain-bound high affinity state of Na,K-ATPase. In Fig. S1 we show a comparison between the transmembrane segments of the $E2(Rb_2)MgF_4$ and ouabain-bound structures of the Na,K-ATPase.

3.3 A model for Rb^+ occlusion in E2P and $E2BeF_x$

To analyze the results of Rb^+ occlusion we used the model shown in Fig. 11, where E represents E2P or $E2BeF_x$. The main purpose of the model, which was first proposed by Forbush [32], was not to obtain quantitative information, but rather to test its consistency and use it as a frame to compare the results obtained with Pi and BeF_x . The model includes species with bound but not occluded Rb^+ ($Rb-E$, $E-Rb$ and $E-Rb_2$, with an open gate), Rb^+ -occluded species ($(Rb)E$, $E(Rb)$ and $E(Rb_2)$, with a closed gate) and a Rb^+ -free occluded state (E_{occ}), which is not capable of binding the cation. The gate only enables the extracellular access for the transported ions since the enzyme is stabilized in the E2 conformation. Therefore, exposure of the sites to the intracellular medium, which would require a transition to the E1 conformation, was omitted in the model. According to the model, the binding of the second Rb^+ requires a change in the position of the Rb^+ bound in the access site to the bottom site. It is also evident, that the Rb^+ bound in the bottom position will only be released after the dissociation of the more superficial one. It is worth of note that, although we are not considering it here, there can be changes in the nature of the phosphoryl (or phosphoryl-like) group bond due to Rb^+ occlusion.

Numerical solutions of the model in Fig. 11 were simultaneously fitted to the results of equilibrium and transient-state experiments (Figs. 7, 9 and 10). Rb_{occ} is composed by the sum of $[(Rb)E]$, $[E(Rb)]$ and 2 times $[E(Rb_2)]$. The model adequately described the results with Pi and BeF_x (see continuous lines in

Fig. 12) for the values of the parameters listed in Table 1, which were obtained with the help of a fitting procedure. Since the number of parameters of the model exceeds that which can be obtained from the experimental information, the individual values of the model cannot be estimated with a reasonable degree of confidence. However, the fitting allowed obtaining a possible set of parameters, which were used to test the predictions of the model. Note that the global fitting did not include Rb^+ deocclusion data in the presence of Pi, which were studied elsewhere [30, 32]. Nonetheless, in Fig. 12C we present the simulated curves according to the model and parameters in Table 1. It can be seen that, as observed by others [30, 32], the time courses predicted two phases of similar amplitude and the decrease of k_2 (Eq. 4) with a $K_{0.5}$ of about $30 \mu\text{M}$ (see inset in Fig. 12C), which compares reasonably with values of $50\text{-}60 \mu\text{M}$ found in the literature.

To further test the ability of the model to explain the experimental results we proceeded as follows: (i) values in Table 1 were used to simulate time courses of Rb^+ occlusion and deocclusion for varying $[\text{Rb}^+]$; (ii) Equation 4 was fitted to the simulated data of Rb^+ deocclusion in the presence of BeF_x and best fitting values of the parameters were plotted in Fig. 9, B and C; (iii) Equation 5 was fitted to the simulated data of the time course of Rb^+ occlusion and best fitting values of the parameters were plotted in Fig. 10, panels B and C for Pi and panels E and F for BeF_x . It can be seen in Figs. 9 and 10 a good agreement between the parameters that best fit the simulated data and those obtained experimentally.

3.3.1 A description of Rb^+ occlusion and deocclusion

Table 2 shows the meaning of the parameters in Equation 3, used to describe equilibrium results, expressed in terms of the parameters of the model presented in Fig. 11. We also included the values calculated according to those in Table 1, which show a good agreement with the values obtained from the empirical fitting using Equation 3. It can be seen that empirical parameters are complex combinations of the rate constants of the model. K_{Rb1} and K_{Rb2} are respectively proportional to the Rb^+ dissociation constants, K_1 and K_2 , but they also depend on the equilibrium of occlusion (K_{occ0} through K_{occ3}) and on the equilibrium constants of cation translocation (K_i and K'_i). According to Table 2, the maximal values of Occ_1 and Occ_2 are E_T and $2 \times E_T$, respectively. The maximal value for Occ_1 is attained when K_{occ1} and $K_{\text{occ2}} \gg 1$, and the maximal value for Occ_2 , when $K_{\text{occ3}} \gg 1$. In the case of E2BeF_x , the empirical value of

Occ_1 ($1.65 \text{ nmol Rb}^+ (\text{mg protein})^{-1}$) is significantly lower than the maximal predicted value ($E_T = 2.3 \text{ nmol (mg protein)}^{-1}$), indicating that $E2\text{BeF}_x$ presents a significant proportion of enzyme species with one Rb^+ bound but not occluded.

Equation 3 predicts sigmoidicity when:

$$\frac{\text{Occ}_2}{K_{\text{Rb}2}} > \frac{\text{Occ}_1}{K_{\text{Rb}1}} \quad \text{Eq. 6}$$

which, according to the model, can be expressed as:

$$2 K_I (1 + K_{\text{occ}0}) K_{\text{occ}3} K_t > K_2 (K_{\text{occ}1} (1 + K_{\text{occ}2}) + K_{\text{occ}2} (1 + K_{\text{occ}1}) K_t) (1 + K_t) \quad \text{Eq. 7}$$

The relationship between the values of K_I and K_2 contributes to but does not determine the shape of the curves. In E2P the occlusion of the first Rb^+ significantly increases the apparent affinity for the second cation. In contrast, in $E2\text{BeF}_x$ the occlusion of one Rb^+ leads to an enzyme form that presents a site with low affinity for the binding and occlusion of the second Rb^+ . This low affinity might either be caused by a high value of the equilibrium constant for the dissociation of Rb^+ from $E\text{-Rb}_2$ (K_2) or by a low concentration of $E\text{-Rb}$ in equilibrium, which implies a high value of $K_{\text{occ}2}$ and/or of K' . The difficulty for the occlusion of the second Rb^+ in $E2\text{BeF}_x$ possibly reflects that of its coupled reaction, i.e. that of E2P shifting from the ground to the transition state.

The release of Rb^+ could be explained according to the *single file* nature of the model [32]: the fast phase might be attributed to the disappearance of species with Rb^+ occluded at the access position, while the slow phase represents the release of the cation that was initially in the bottom site and had to move closer to the gate. The rate of Rb^+ release from the bottom site is reduced by the presence of Rb^+ in the medium that tends to occupy the access site (Fig. S2). In the case of $E2\text{BeF}_x$, this effect simultaneously explains the low affinity for Rb^+ of both the decrease in k_2 (Eq. 4) and the second component in the equilibrium results ($K_{\text{Rb}2}$). The model can also explain the tendency of the amplitudes of the slow and fast phases to be similar with the increase in $[\text{Rb}^+]$ (A_1 and A_2 in Fig. 9B), a condition in which the equilibrium will be shifted to the enzyme species holding two occluded Rb^+ .

During Rb^+ occlusion by E2P and $E2\text{BeF}_x$ the very fast phase (A_0 in Equation 5) is explained by the existence of the open-enzyme form, E, able to rapidly bind and occlude one Rb^+ at the access site

forming (Rb)E. Thus, the size of this component is proportional to the amount of E, being higher for E2P (Fig. 10). Besides, the slow phase is composed by (i) the formation of species with 2 occluded Rb^+ , which is limited by the rate at which the Rb^+ at the access site moves to the bottom site, and (ii) the rate of new formation of open enzyme from E_{occ} , governed by $k_{-\text{occ}0}$, which was predicted by Forbush in his *Flickering Gate Model* [34].

4. Final Remarks

In this work we have characterized the properties of the E2P-like state, $E2\text{BeF}_x$, and compared them with those of E2P. Results show that:

- BeF_x is the only metal-fluoride compound that, like Pi, increases the RH421 signal upon binding to the Na,K-ATPase, which favors the idea that $E2\text{BeF}_x$ mimics the E2P ground state.
- A conformational-selection mechanism seems a simpler explanation for the binding of Pi and Pi-analogs to the Na,K-ATPase.
- It is normally assumed that the occlusion of two K^+ accelerates the dephosphorylation more than 100 times. The difficulty for the occlusion of the second Rb^+ in $E2\text{BeF}_x$ is probably because this reaction triggers the first change in the phosphoryl group that leads to dephosphorylation. As this change is hindered in the $E2\text{BeF}_x$ complex, this interferes with the reaction stages that lead to the occlusion of the second cation.
- The rates of Rb^+ occlusion and deocclusion in the presence of BeF_x are higher than those observed for $E2\text{MgF}_x$ (E2P product state) and for $E2\text{Mg-vanadate}$ (E2P transition state) suggesting the existence of a more open access to the cation sites as expected for the ground state.

Our results provide functional information that matches the structure proposed for this state in other P-type ATPases. Although the use of metal fluoride compounds provides essential information to understanding the dephosphorylation mechanism, it is important to pay attention to the kinetic differences found between E2P and $E2\text{BeF}_x$ when analyzing crystal structures.

Acknowledgements: We thank Ms. Angielina Damgaard and Ms. Birthe B. Jensen from the Department of Biophysics of the University of Aarhus (Denmark) for preparing the Na,K-ATPase. This work was supported by Agencia Nacional de Promoción Científica y Tecnológica [PICT 2012-2014, 1053], Consejo Nacional de Investigaciones Científicas y Técnicas [PIP 11220150100250CO], and Universidad de Buenos Aires [UBACyT 2014-2017, 20020130100302BA].

References

- [1] W. Kuhlbrandt, Biology, structure and mechanism of P-type ATPases, *Nat. Rev. Mol. Cell Biol.*, 5 (2004) 282-295.
- [2] A.J. Murphy, J.C. Hoover, Inhibition of the Na,K-ATPase by fluoride. Parallels with its inhibition of the sarcoplasmic reticulum CaATPase, *J. Biol. Chem.*, 267 (1992) 16995-16700.
- [3] S. Danko, K. Yamasaki, T. Daiho, H. Suzuki, Distinct natures of beryllium fluoride-bound, aluminum fluoride-bound, and magnesium fluoride-bound stable analogues of an ADP-insensitive phosphoenzyme intermediate of sarcoplasmic reticulum Ca²⁺-ATPase: changes in catalytic and transport sites during phosphoenzyme hydrolysis, *J. Biol. Chem.*, 279 (2004) 14991-14998.
- [4] J.D. Clausen, D.B. McIntosh, D.G. Woolley, J.P. Andersen, Modulatory ATP binding affinity in intermediate states of E2P dephosphorylation of sarcoplasmic reticulum Ca²⁺-ATPase, *J. Biol. Chem.*, 286 (2011) 11792-11802.
- [5] C. Toyoshima, H. Nomura, T. Tsuda, Lumenal gating mechanism revealed in calcium pump crystal structures with phosphate analogues, *Nature*, 432 (2004) 361-368.
- [6] T. Shinoda, H. Ogawa, F. Cornelius, C. Toyoshima, Crystal structure of the sodium–potassium pump at 2.4 Å resolution, *Nature*, 459 (2009) 446.
- [7] J.P. Morth, B.P. Pedersen, M.S. Toustrup-Jensen, T.L.M. Sørensen, J. Petersen, J.P. Andersen, B. Vilsen, P. Nissen, Crystal structure of the sodium–potassium pump, *Nature*, 450 (2007) 1043.
- [8] C. Toyoshima, Structural aspects of ion pumping by Ca²⁺-ATPase of sarcoplasmic reticulum, *Arch. Biochem. Biophys.*, 476 (2008) 3-11.
- [9] K. Abe, K. Tani, Y. Fujiyoshi, Structural and functional characterization of H⁺, K⁺-ATPase with bound fluorinated phosphate analogs, *J. Struct. Biol.*, 170 (2010) 60-68.
- [10] K. Abe, K. Tani, T. Friedrich, Y. Fujiyoshi, Cryo-EM structure of gastric H⁺,K⁺-ATPase with a single occupied cation-binding site, *Proc. Natl. Acad. Sci. U. S. A.*, 109 (2012) 18401-18406.
- [11] R.C. Rossi, S.B. Kaufman, R.M. Gonzalez Lebrero, J.G. Norby, P.J. Garrahan, An attachment for nondestructive, fast quenching of samples in rapid-mixing experiments, *Anal. Biochem.*, 270 (1999) 276-285.
- [12] M.R. Montes, J.L. Monti, R.C. Rossi, E₂→E₁ transition and Rb(+) release induced by Na(+) in the Na(+)/K(+)-ATPase. Vanadate as a tool to investigate the interaction between Rb(+) and E₂, *Biochim. Biophys. Acta*, 1818 (2012) 2087-2093.

- [13] M.R. Montes, M.S. Ferreira-Gomes, M. Centeno, R.C. Rossi, The E2P-like state induced by magnesium fluoride complexes in the Na,K-ATPase. Kinetics of formation and interaction with Rb(+), *Biochim. Biophys. Acta*, 1848 (2015) 1514-1523.
- [14] I. Klodos, M. Esmann, R.L. Post, Large-scale preparation of sodium-potassium ATPase from kidney outer medulla, *Kidney Int.*, 62 (2002) 2097-2100.
- [15] R.E. Mesmer, C.F. Baes, Fluoride complexes of beryllium(II) in aqueous media, *Inorg. Chem.*, 8 (1969) 618-626.
- [16] M.R. Montes, R.M. Gonzalez-Lebrero, P.J. Garrahan, R.C. Rossi, Eosin fluorescence changes during Rb⁺ occlusion in the Na⁺/K⁺-ATPase, *Biochemistry*, 45 (2006) 13093-13100.
- [17] J.C. Skou, M. Esmann, Eosin, a fluorescent probe of ATP binding to the (Na⁺ + K⁺)-ATPase, *Biochim. Biophys. Acta*, 647 (1981) 232-240.
- [18] N.U. Fedosova, F. Cornelius, I. Klodos, E2P Phosphoforms of Na,K-ATPase. I. Comparison of Phosphointermediates Formed from ATP and Pi by Their Reactivity toward Hydroxylamine and Vanadate, *Biochemistry*, 37 (1998) 13634-13642.
- [19] K.P. Burnham, D.R. Anderson, *Model Selection and Multimodel Inference*, 2 ed., Springer-Verlag, New York, 2002.
- [20] S. Hoops, S. Sahle, R. Gauges, C. Lee, J. Pahle, N. Simus, M. Singhal, L. Xu, P. Mendes, U. Kummer, COPASI--a COMplex PATHway SIMulator, *Bioinformatics*, 22 (2006) 3067-3074.
- [21] C. Toyoshima, Y. Norimatsu, S. Iwasawa, T. Tsuda, H. Ogawa, How processing of aspartylphosphate is coupled to lumenal gating of the ion pathway in the calcium pump, *Proc. Natl. Acad. Sci. U. S. A.*, 104 (2007) 19831-19836.
- [22] I. Klodos, N.U. Fedosova, L. Plesner, Influence of intramembrane electric charge on Na,K-ATPase, *J. Biol. Chem.*, 270 (1995) 4244-4254.
- [23] N.U. Fedosova, F. Cornelius, I. Klodos, E2P phosphoforms of Na,K-ATPase. I. Comparison of phosphointermediates formed from ATP and Pi by their reactivity toward hydroxylamine and vanadate, *Biochemistry*, 37 (1998) 13634-13642.
- [24] A. Garcia, P.R. Prapat, C. Lupfert, F. Cornelius, D. Jacquemin, B. Lev, T.W. Allen, R.J. Clarke, The voltage-sensitive dye RH421 detects a Na(+),K(+)-ATPase conformational change at the membrane surface, *Biochim. Biophys. Acta*, 1859 (2017) 813-823.
- [25] S.L. Myers, F. Cornelius, H.J. Apell, R.J. Clarke, Kinetics of K(+) occlusion by the phosphoenzyme of the Na(+),K(+)-ATPase, *Biophys. J.*, 100 (2011) 70-79.
- [26] M. Pedersen, M. Roudna, S. Beutner, M. Birnes, B. Reifers, H.D. Martin, H.J. Apell, Detection of charge movements in ion pumps by a family of styryl dyes, *J. Membr. Biol.*, 185 (2002) 221-236.
- [27] F. Cornelius, N.U. Fedosova, I. Klodos, E2P phosphoforms of Na,K-ATPase. II. Interaction of substrate and cation-binding sites in Pi phosphorylation of Na,K-ATPase, *Biochemistry*, 37 (1998) 16686-16696.
- [28] F. Cornelius, Y.A. Mahmmoud, C. Toyoshima, Metal fluoride complexes of Na,K-ATPase: characterization of fluoride-stabilized phosphoenzyme analogues and their interaction with cardiotonic steroids, *J. Biol. Chem.*, 286 (2011) 29882-29892.
- [29] A.D. Vogt, E. Di Cera, Conformational selection or induced fit? A critical appraisal of the kinetic mechanism, *Biochemistry*, 51 (2012) 5894-5902.

- [30] R.M. Gonzalez-Lebrero, S.B. Kaufman, P.J. Garrahan, R.C. Rossi, The pathway for spontaneous occlusion of Rb⁺ in the Na⁺/K⁺-ATPase, *Biochemistry*, 47 (2008) 6073-6080.
- [31] B. Forbush, 3rd, Rapid ⁸⁶Rb release from an occluded state of the Na,K-pump reflects the rate of dephosphorylation or dearsenylation, *J. Biol. Chem.*, 263 (1988) 7961-7969.
- [32] B. Forbush, 3rd, Rapid release of ⁴²K or ⁸⁶Rb from two distinct transport sites on the Na,K-pump in the presence of Pi or vanadate, *J. Biol. Chem.*, 262 (1987) 11116-11127.
- [33] R.M. Gonzalez-Lebrero, S.B. Kaufman, M.R. Montes, J.G. Norby, P.J. Garrahan, R.C. Rossi, The Occlusion of Rb(+) in the Na(+)/K(+)-ATPase. I. The identity of occluded states formed by the physiological or the direct routes: occlusion/deocclusion kinetics through the direct route, *J. Biol. Chem.*, 277 (2002) 5910-5921.
- [34] B. Forbush, Occluded Ions and Na,K-ATPase, in: J.C. Skou, J.G. Norby, A.B. Maunsbach, M. Esmann (Eds.) *The Na⁺,K⁺-Pump, Part A: Molecular Aspects*, Alan R. Liss, Inc., New York, 1988, pp. 229-248.
- [35] S.J.D. Karlsh, W.D. Stein, Passive rubidium fluxes mediated by Na-K-ATPase reconstituted into phospholipid vesicles when ATP- and phosphate-free, *The Journal of Physiology*, 328 (1982) 295-316.
- [36] M. Esmann, Influence of Na⁺ on conformational states in membrane-bound renal Na,K-ATPase, *Biochemistry*, 33 (1994) 8558-8565.
- [37] P.A. Humphrey, C. Lupfert, H.J. Apell, F. Cornelius, R.J. Clarke, Mechanism of the rate-determining step of the Na(+),K(+)-ATPase pump cycle, *Biochemistry*, 41 (2002) 9496-9507.
- [38] S.B. Kaufman, R.M. Gonzalez-Lebrero, R.C. Rossi, P.J. Garrahan, Binding of a single Rb⁺ increases Na⁺/K⁺-ATPase, activating dephosphorylation without stoichiometric occlusion, *J. Biol. Chem.*, 281 (2006) 15721-15726.
- [39] L. Beauge, Breakdown of Na⁺/K⁺-exchanging ATPase phosphoenzymes formed from ATP and from inorganic phosphate during Na⁺-ATPase activity, *Eur. J. Biochem.*, 268 (2001) 5627-5632.
- [40] R.L. Post, G. Toda, F.N. Rogers, Phosphorylation by inorganic phosphate of sodium plus potassium ion transport adenosine triphosphatase. Four reactive states, *J. Biol. Chem.*, 250 (1975) 691-701.
- [41] C. Olesen, M. Picard, A.M. Winther, C. Gyruup, J.P. Morth, C. Oxvig, J.V. Moller, P. Nissen, The structural basis of calcium transport by the calcium pump, *Nature*, 450 (2007) 1036-1042.
- [42] L. Yatime, M. Laursen, J.P. Morth, M. Esmann, P. Nissen, N.U. Fedosova, Structural insights into the high affinity binding of cardiotonic steroids to the Na⁺,K⁺-ATPase, *J. Struct. Biol.*, 174 (2011) 296-306.

Figure legends

Figure 1: A simplified version of the Albers-Post model for the functioning of Na,K-ATPase. The shaded area represents the dephosphorylation reaction due to K^+ binding that occurs through a series of consecutive states.

Figure 2: Effects of Pi, BeSO₄ and ImF on eosin fluorescence. Fluorescence was measured at 540 nm for a Na,K-ATPase suspension in the presence of 0.4 μ M eosin with (A) 3 mM MgCl₂ as a function of [Pi], (B) 0.3 mM MgCl₂ and 2 mM ImF as a function of [BeSO₄] and (C) 0.3 mM MgCl₂ and 100 μ M BeSO₄ as a function of [ImF]. Continuous lines are graphics of the equations described in the main text.

Figure 3: RH421 fluorescence change in rapid mixing stopped-flow assays. The enzyme was mixed with Pi, vanadate, MgF_x, AlF_x or BeF_x. Experiments were performed with (final concentrations) 45 μ g protein ml⁻¹ in the presence of 0.3 μ M RH421, 3 mM MgCl₂ and 5.65 mM Pi, 0.2 mM vanadate, 6 mM ImF (MgF_x), 0.3 mM AlCl₃ and 2 mM ImF (AlF_x), or 100 μ M BeSO₄ and 2 mM ImF (BeF_x).

Figure 4: Effects of Pi and BeF_x on the time courses of RH421 fluorescence change. Experiments were performed in the rapid-mixing stopped-flow spectrofluorometer with 45 μ g protein ml⁻¹ in the presence of (A) 0.05 to 1.00 mM Pi with 3 mM MgCl₂, or (B) 5 to 200 μ M BeSO₄ with 0.3 mM MgCl₂ and 2 mM ImF.

Figure 5. Observed rate constant of the RH421 fluorescence change. k_{obs} (values \pm 1 S.E.) for varying concentrations of (A) Pi or (B) BeF₃⁻ were obtained by fitting Equation 1 to the kinetic traces shown in Fig. 4. Continuous and dashed lines represent, respectively, the independent and global fittings of Equation 2 to the k_{obs} values, for the parameters shown in the table. In the table, values are expressed \pm standard errors; otherwise, they are not significant. The concentration of BeF₃⁻ was calculated from the total concentration of beryllium and fluoride according to Mesmer and Baes [15].

Figure 6. Effect of Na⁺ on eosin fluorescence in the presence of Pi or BeF_x. The suspension of Na,K-ATPase, incubated with Pi or BeF_x, was mixed with a medium containing NaCl, and the time courses were recorded for at least 200 s. Final concentrations were 45 μ g protein ml⁻¹, 0.32 μ M eosin, 60 mM NaCl, and either 3 mM MgCl₂ and 5 mM Pi, or 0.3 mM MgCl₂, 2 mM ImF and 100 μ M BeSO₄.

Figure 7. Equilibrium values of occluded Rb⁺. Na,K-ATPase (45 μ g protein ml⁻¹) was incubated with varying concentrations of Rb⁺ in the presence of (A) 5 mM Pi and 0.5 mM MgCl₂ or (B) BeF_x (2 mM ImF, 50 μ M BeSO₄ and 0.3 mM MgCl₂). The insets show a detail of Rb_{occ} values at low Rb⁺ concentrations. Continuous lines represent the best fitting of Equation 3 to the data.

Figure 8: Effects of BeF_x on the kinetics of Rb⁺ release. The Rb⁺ occluded states were formed incubating the enzyme with ⁸⁶Rb⁺ in the presence (●) or absence (○) of BeF_x. At time = 0, this suspension was mixed with enough of a similar medium, but lacking ⁸⁶Rb⁺ to cause a 20-fold isotopic dilution of ⁸⁶Rb⁺. Final concentrations were: 45 μ g protein ml⁻¹ and 0.1 mM Rb⁺; and 0.3 mM MgCl₂, 2 mM ImF, and 50 μ M BeSO₄ when BeF_x was present.

Figure 9. Time course of Rb⁺ release from E2BeF_x(Rb_n) formed at different [Rb⁺]. A, occluded ⁸⁶Rb⁺ remaining after a 20-fold isotopic dilution. The inset shows a detail of the first 25 seconds of the time courses. Experiments were performed with (final concentrations) 45 μg protein ml⁻¹, 0.3 mM MgCl₂, 2 mM ImF, 50 μM BeSO₄, and the following concentrations of Rb⁺: 30 μM (△), 100 μM (▲), 1000 μM (□) and 5000 μM (●). Continuous lines represent the best fitting of Equation 4 to the data. The best fitting values of the parameters are shown in B and C. Vertical bars are ± 1 S.E. Dashed lines are plots of the best fitting values of Equation 4 fitted to data simulated according to the model shown in Fig. 11 using the parameters listed in Table 1.

Figure 10. Time course of Rb⁺ occlusion. Na,K-ATPase (45 μg protein ml⁻¹) in the presence of (A) 5 mM Pi and 0.5 mM MgCl₂ or (D) BeF_x (2 mM ImF, 50 μM BeSO₄ and 0.3 mM MgCl₂), was mixed with 30 μM (△), 100 μM (▲), 2000 μM (○) and 5000 μM (●) Rb⁺ (final concentrations). Continuous lines represent the best fit of Equation 5 to the data. The best fitting values of the parameters (± 1 S.E.) are shown in panels B and C for Pi, and E and F for BeF_x. Dashed lines are plots of the best fitting values of Equation 5 fitted to data that were simulated according to the model shown in Fig. 11 using the parameters listed in Table 1.

Figure 11. A model for Rb⁺ occlusion. All E forms stand for E2P or E2BeF_x. The boxes represent the Rb-occlusion cavity of the enzyme, which is separated from the medium by a gate. Binding and release of Rb⁺ can only take place when the gate is open. Boxes with a closed gate correspond to occluded states.

Figure 12. Fitting of the model in Fig. 11. The model was simultaneously fitted to the experimental data presented in Figs. 7, 9 and 10. Symbols are experimental results and continuous lines are the plot of the values simulated using the model in Fig. 11 for the parameters values shown in Table 1. Panels A and B: occluded Rb⁺ in equilibrium; panels C and D: kinetics of Rb⁺ release; panels E and F: kinetics of Rb⁺ occlusion. In panels D, E and F, symbols indicate the following Rb⁺ concentrations: 30 μM (△), 100 μM (▲), 1000 μM (□), 2000 μM (○) and 5000 μM (●). The insets in panels C and D show the value of *k*₂ obtained by fitting Equation 4 to simulated data of Rb⁺ release.

Table 1: Best global fitting values of the parameters of the model shown in Fig. 11 to results from equilibrium and transient experiments of occluded Rb⁺.

Parameter	E2P	E2BeF _x	
k_1	4.7	3.2	$\mu\text{M}^{-1} \text{s}^{-1}$
k_{-1}	3700	400	s^{-1}
k_2	4.3	1.2	$\mu\text{M}^{-1} \text{s}^{-1}$
k_{-2}	94	6500	s^{-1}
k_{occ0}	0.083	0.10 ± 0.02	s^{-1}
k_{-occ0}	0.10	0.036 ± 0.004	s^{-1}
k_{occ1}	35	1.0 ± 0.4	s^{-1}
k_{-occ1}	11	0.24 ± 0.03	s^{-1}
k_{occ2}	42	0.54	s^{-1}
k_{-occ2}	1.2	0.0055 ± 0.0011	s^{-1}
k_{occ3}	310	76	s^{-1}
k_{-occ3}	12	0.60 ± 0.22	s^{-1}
k_t	0.019	0.0000038	s^{-1}
k_{-t}	0.0027	0.0000068	s^{-1}
k'_t	1.7	0.025	s^{-1}
k'_{-t}	2.8	1.0	s^{-1}

The value of E_T used in the fitting procedure was $2.38 \text{ nmol (mg protein)}^{-1}$. When applicable, values are expressed \pm standard errors. Otherwise values are not significant.

Table 2: Parameters in Equation 3 in terms of constants from the model in Fig. 11.

Empirical parameters	Meaning	Calculated from the values in Table 1		
		Pi	BeF _x	units
K _{Rb1}	$\frac{K_1(1 + K_{occ0}) K_{occ2} K_t}{K_{occ1} (1 + K_{occ2}) + K_{occ2} (1 + K_{occ1}) K_t}$	0.054 ± 0.017	0.0602 ± 0.0038	mM
K _{Rb2}	$\frac{K_2 (K_{occ1} (1 + K_{occ2}) + K_{occ2} (1 + K_{occ1}) K_t)}{K_{occ1} (1 + K_{occ3})}$	0.0349 ± 0.0093	12.9 ± 5.0	mM
Occ ₁	$\frac{E_T K_{occ1} K_{occ2} (1 + K_t)}{K_{occ1} (1 + K_{occ2}) + K_{occ2} (1 + K_{occ1}) K_t}$	2.2 ± 1.4	2.060 ± 0.056	nmol Rb ⁺ (mg protein) ⁻¹
Occ ₂	$\frac{2 E_T K_{occ3}}{1 + K_{occ3}}$	4.574 ± 0.074	4.72 ± 0.60	nmol Rb ⁺ (mg protein) ⁻¹

Where $K_1=k_{-1}/k_1$, $K_2=k_{-2}/k_2$, $K_t=k_{-t}/k_t$, $K'_t=k'_{-t}/k'_t$, $K_{occ0}=k_{occ0}/k_{-occ0}$, $K_{occ1}=k_{occ1}/k_{-occ1}$, $K_{occ2}=k_{occ2}/k_{-occ2}$ and $K_{occ3}=k_{occ3}/k_{-occ3}$. E_T: total enzyme. K'_t was calculated as $K_{occ1}K_t/K_{occ2}$ using the thermodynamic equivalence of pathways.

HIGHLIGHTS

Formation of E2BeF_x and E2P may be explained by a conformational selection mechanism

Like Pi, BeF_x increases RH421 fluorescence signal upon binding to Na,K-ATPase

The occlusion of Rb⁺ by E2P displays positive cooperativity

The occlusion of Rb⁺ by E2BeF_x displays negative cooperativity

E2BeF_x seems to present an open extracellular access

ACCEPTED MANUSCRIPT

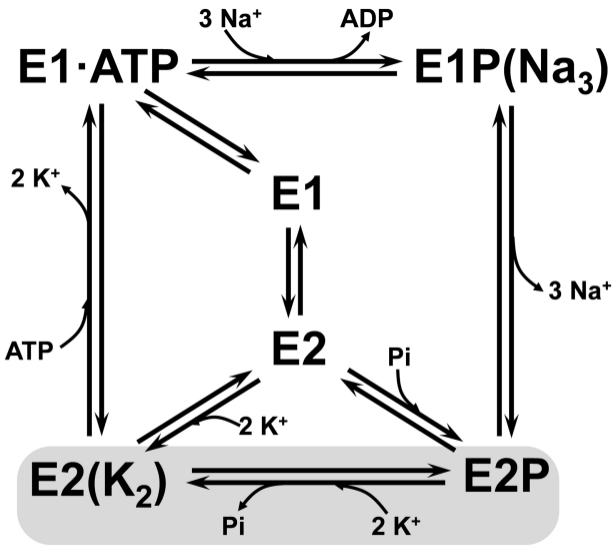


Figure 1

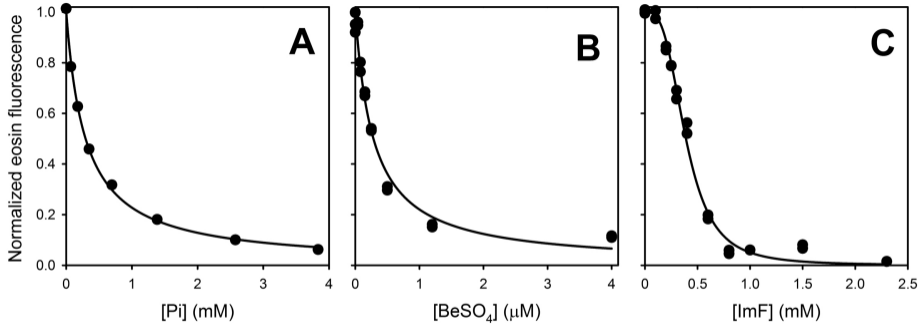


Figure 2

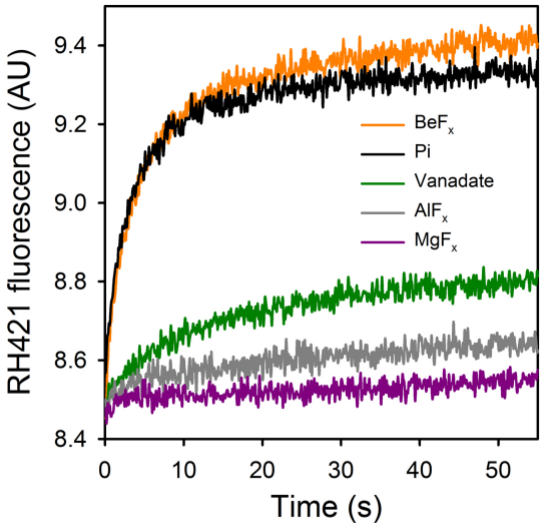
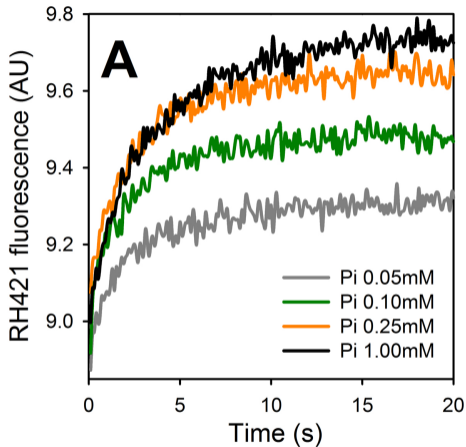


Figure 3

Pi



BeF_x

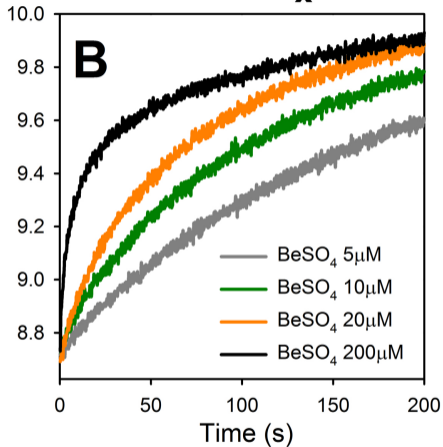
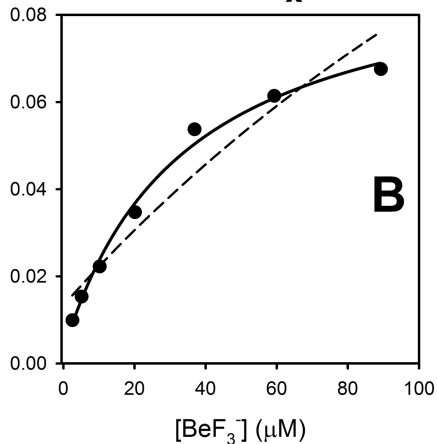
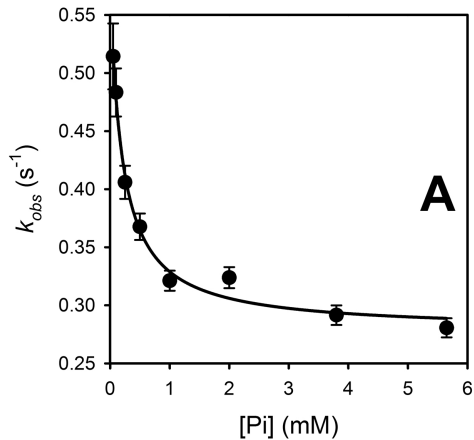


Figure 4

Pi**BeF_x**

	Independent fittings		Global fitting	
	Pi	BeF ₃ ⁻	Pi	BeF ₃ ⁻
k_r (s ⁻¹)	0.2783 ± 0.0079	0.094 ± 0.026	0.2782 ± 0.0067	0.2782 ± 0.0067
k_{-r} (s ⁻¹)	206	158	861	861
k_{on} (μM ⁻¹ s ⁻¹)	1.0	4.7	4.2	3.0
k_{off} (s ⁻¹)	0.574	0.0027	0.574 ± 0.018	0.0133 ± 0.0054

Figure 5

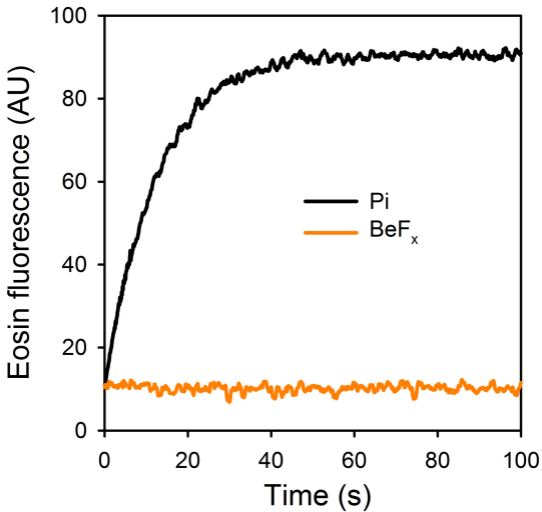
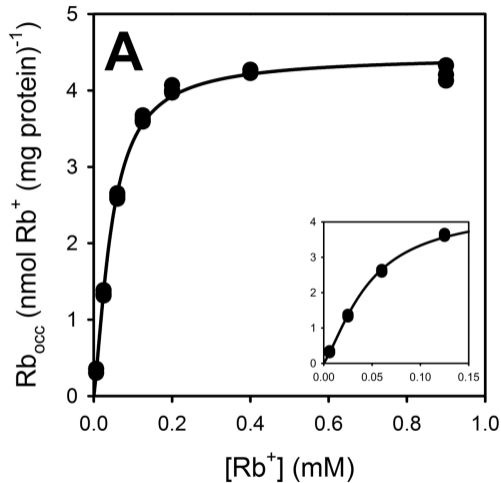


Figure 6

Pi



BeF_x

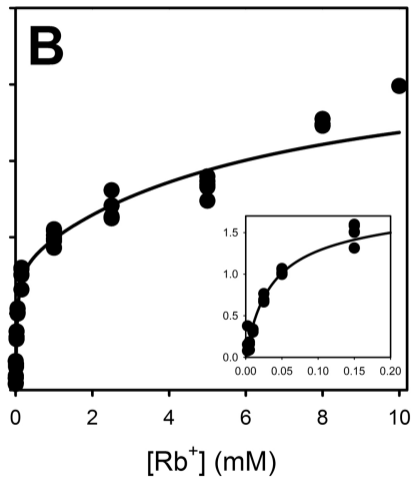


Figure 7

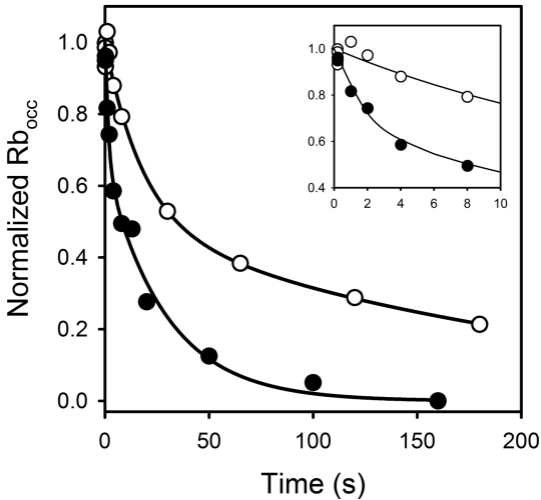


Figure 8

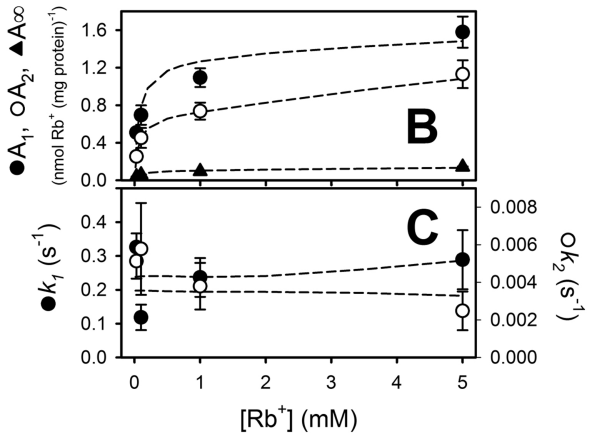
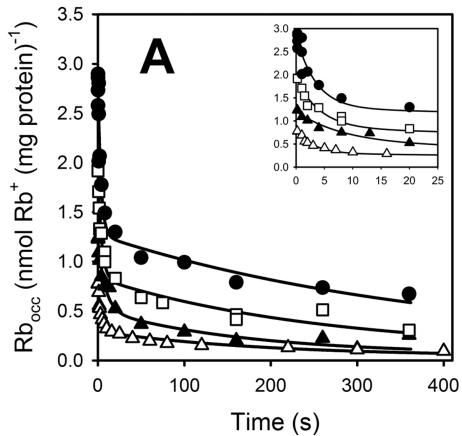


Figure 9

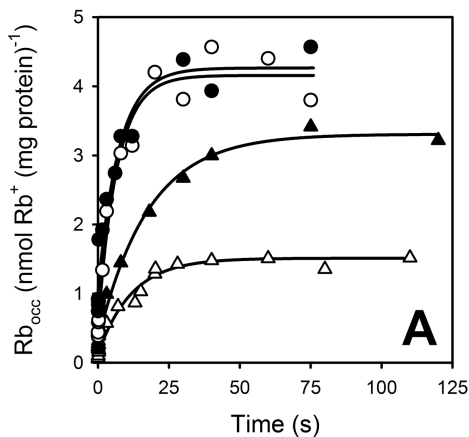
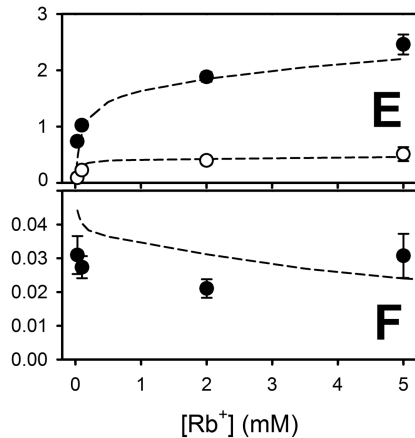
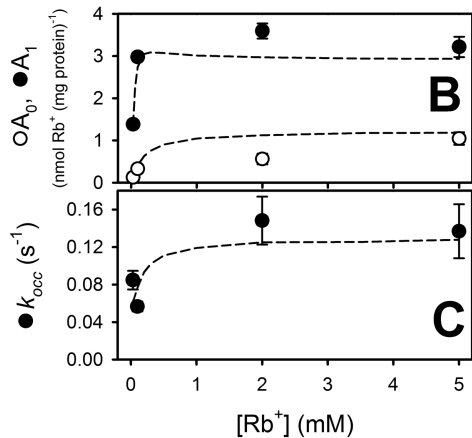
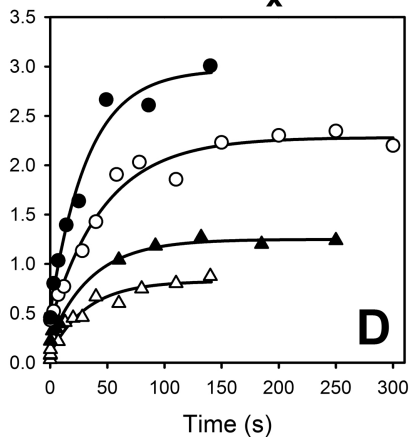
Pi**BeF_x**

Figure 10

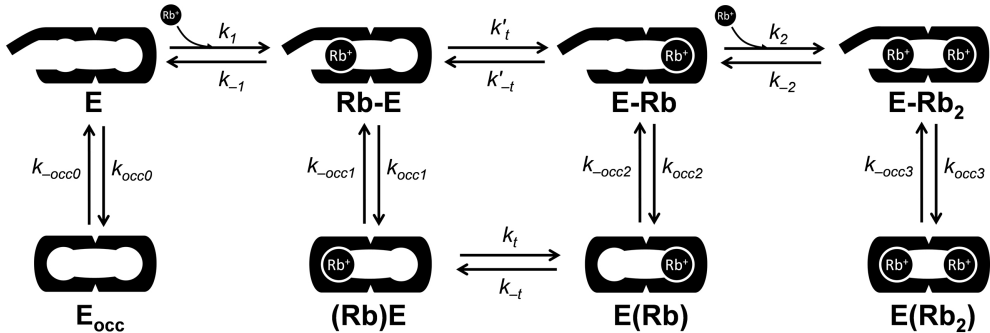


Figure 11

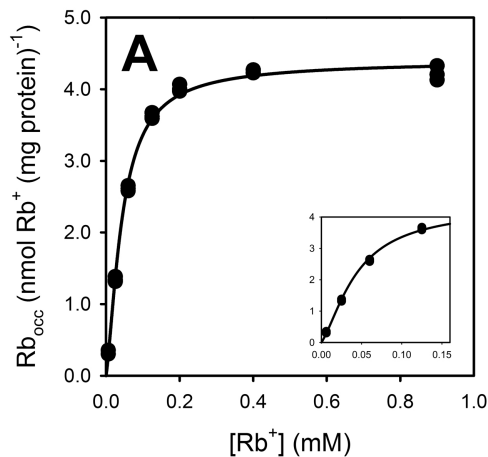
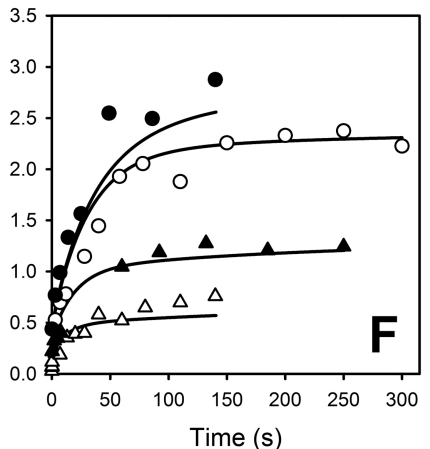
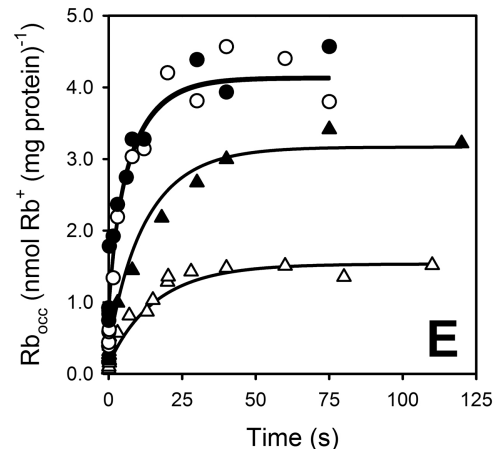
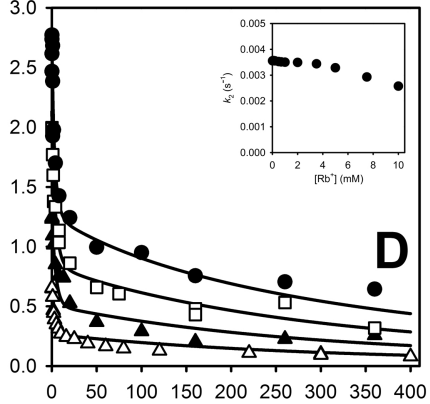
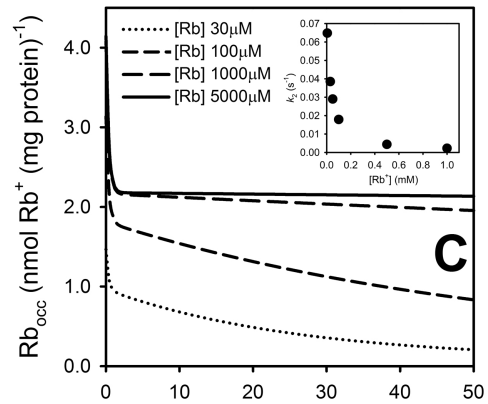
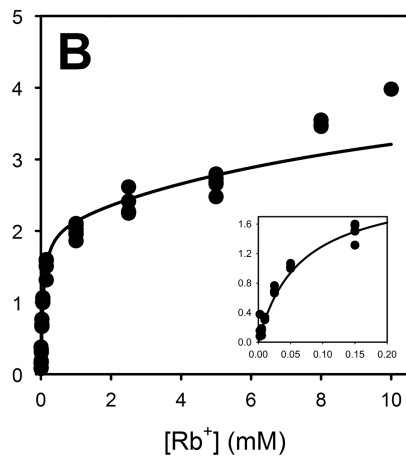
Pi**BeF_x**

Figure 12